

1 **Stability test of novel combined formulated dry powder inhalation system**  
2 **containing antibiotic: Physical characterization and *in vitro-in silico* lung**  
3 **deposition results**

4 Edit Benke<sup>a</sup>, Árpád Farkas<sup>b</sup>, Imre Balásházy<sup>b</sup>, Piroska Szabó-Révész<sup>a</sup>, Rita Ambrus<sup>a\*</sup>

5 <sup>a</sup> Institute of Pharmaceutical Technology and Regulatory Affairs, University of Szeged, Szeged,  
6 Hungary

7 <sup>b</sup> Centre for Energy Research, Hungarian Academy of Sciences, Budapest, Hungary

8 \*Corresponding author:

9 Dr. Habil. Rita Ambrus PhD

10 e-mail: [arita@pharm.u-szeged.hu](mailto:arita@pharm.u-szeged.hu)

11 Tel: +36-62-545-572

12

## Abstract

**Objective:** The aim was to study the stability of dry powder inhaler (DPI) formulations containing antibiotic with different preparation ways -carrier-based, carrier-free, and novel combined formulation - and thereby to compare their physicochemical and *in vitro-in silico* aerodynamical properties before and after storage.

**Significance:** Presenting a novel combined technology in the field of DPI formulation including the carrier-based and carrier-free methods, **it is the most important reason** to introduce this stable formulation for the further development of DPIs.

**Methods:** The structure, the residual solvent content, the interparticle interactions, the particle size distribution and the morphology of the samples were studied. The aerodynamic values were determined based on the Cascade Impactor *in vitro* lung model. We tested the *in silico* behaviour of the novel combined formulated samples before and during storage.

**Results:** The physical measurements showed that the novel combined formulated sample was the most favourable. It was found that thanks to the formulation technique and the use of magnesium stearate have a beneficial effect on the stability compare with the carrier-based formulation without magnesium stearate and carrier-free formulations. The results of *in vitro* and *in silico* lung models were consistent with the physical results, so the highest deposition was found for the novel combined formulated sample during the storage.

**Conclusion:** It can be established that after the storage a novel combined formulated DPI contained amorphous drug to have around 2.5  $\mu\text{m}$  mass median aerodynamic diameter and nearly 50 % fine particle fraction predicted high lung deposition *in silico* also.

**Keywords:** novel combined formulation, pulmonary drug delivery, ciprofloxacin hydrochloride, sodium stearate, magnesium stearate, *in silico* assessment, interparticle interactions

## 1. Introduction

1 Cystic fibrosis (CF) is an autosomal recessive hereditary disease, caused by mutations in the  
2 gene that encodes the cystic fibrosis transmembrane conductance regulator (CFTR) protein  
3 [1,2]. Due to the mutation, ion transports are modified through the membrane of airway  
4 epithelial cells. As a result, the pH of the airway surface liquid is lowered, the mucus is  
5 concentrated, mucociliary clearance efficiency is decreased, and the inflammation causes  
6 mucin hypersecretion, which promotes bacterial infection [3–6]. “Polymicrobial” infection –  
7 which is defined as an individual patient at a particular point of time infected with a number of  
8 different organisms – is characteristic of CF. The most typical bacteria are: *Pseudomonas*  
9 *aeruginosa*, *Haemophilus influenzae* and *Burkholderia cepacia* (Gram-negatives);  
10 *Staphylococcus aureus* (Gram-positive). *Haemophilus influenzae* and *Staphylococcus aureus*  
11 cause the early infections of CF respiratory tract, then *Pseudomonas aeruginosa* becomes the  
12 most significant pathogen in adulthood [7]. In CF more effective anti-infective and anti-  
13 inflammatory treatments are required to control ongoing inflammation, tissue destruction, and  
14 exacerbations. Therefore the formulation of potent inhaled agents would offer significant  
15 benefits for the prevention and treatment of pulmonary bacterial infections. The key challenges  
16 of the therapy for airway inflammation, structural changes and mucociliary dysfunction are  
17 opportunities for novel inhaled drug formulations [8,9].

19 Ciprofloxacin hydrochloride is the hydrochloride salt form of ciprofloxacin. This drug is a  
20 second generation fluoroquinolone antibiotic, which is a fluorinated derivative of nalidixic acid  
21 [10,11]. Ciprofloxacin is effective against both Gram-positive and Gram-negative  
22 microorganisms. In point of its mechanism of action, the main target is the bacterial enzymes  
23 DNA gyrase (topoisomerase II) in Gram-negative bacteria and topoisomerase IV in Gram-  
24 positive bacteria [12,13]. Therefore, it may be used for respiratory bacterial infections in  
25 patients with CF [14].

1 Drugs (e.g. antibiotics) can be delivered via the pulmonary route for the purpose of achieving  
2 local and systemic effects. This type of drug delivery has many advantages. For example, it  
3 should be noted that by circumventing the gastrointestinal tract, the drugs reach the  $C_{max}$  value  
4 in the blood within approximately 1-3 minutes [15]. By avoiding the first-pass effect of the liver  
5 and the enzymatic inactivation of the gastrointestinal system as metabolic pathways, the use of  
6 lower doses of active agents is sufficient to induce the same therapeutic effect. Thus, the side  
7 effects profile could be modified. In addition, pulmonary drug delivery is a non-invasive  
8 therapeutic procedure, which does not cause pain or tissue damage [16,17]. However, at present  
9 only three inhaled antibiotics (tobramycin, aztreonam and colistimethate (sodium)) are on the  
10 market [18]. The use of the dry powder inhalers (DPIs) offers outstandingly many benefits:  
11 propellant-free, easy to use, portability, increased stability, less need for patient coordination,  
12 etc. [19–21].

13 The specialized literature fundamentally separates carrier-based, and carrier-free systems based  
14 on the formulation of DPI systems. Both formulations have advantages and disadvantages. Most  
15 of the DPIs available on the market are made with carrier-based formulation, which involves  
16 applying the active ingredient particles to the surface of a large carrier particle by forming an  
17 interactive physical mixture. The use of carriers is an advantage in the case of active ingredients  
18 that have a strong cohesive property, the flow properties of the composition are improved,  
19 applying of the small doses of the active substance could be easier by dilution with carrier, and  
20 the taste of the carrier confirms successful inhalation by the patient [22–24]. However, most of  
21 these compositions do not yet have outstanding lung deposition. These formulations have an  
22 average of 20-30 % fine particle fraction (FPF), meaning that the drug reaches the deeper layers  
23 of the lungs in a low percentage [25]. In the case of carrier-free DPI systems, the use of special  
24 excipients (e.g. L-leucine) and technologies (e.g. co-spray-drying) makes the application of a  
25 large carrier avoidable. Generally, these systems have low density and special morphology.

1 However, they have around 50-60 % FPF results due to the apparent high cohesive properties  
2 between the active ingredient's particles [26,27]. Many publications deal with the development  
3 of DPI containing ciprofloxacin or ciprofloxacin hydrochloride [12,28–33]. A serious challenge  
4 of our previous work was using the benefits of these two formulations (applying 1:10 ratio and  
5 current inhaled antibiotics are ~100 mg), the novel combined formulation (a co-spray-dried  
6 drug blended with surface modified lactose) produced by us resulted in a higher FPF value than  
7 the carrier-based and carrier-free DPI formulations [18].

8 The aim of the present work was – on the basis of the aforementioned publication [18] – the  
9 stability testing of the carrier-based formulation; carrier-free formulation and novel combined  
10 formulation DPI systems, which contain ciprofloxacin hydrochloride. Before and after the  
11 storage we investigated the morphology, particle size and structure changes of prepared  
12 formulations, as well as the modification of interparticle interactions, and mainly how these  
13 physical changes influence the *in vitro* aerodynamic parameters. Furthermore, our aim was to  
14 carry out computer simulations of lung deposition (from now on termed as *in silico* modeling)  
15 at the stability test times with the novel combined formulated samples and compare these results  
16 with the *in vitro* aerodynamic results.

17

18

## 2. Materials and methods

### 19 2.1. Materials

20 Micronized ciprofloxacin hydrochloride ( $\mu$ CIP) (D50: 5.09  $\mu$ m), was kindly provided by Teva  
21 Pharmaceutical Works Ltd. (Debrecen, Hungary). Lactose monohydrate, Inhalac<sup>®</sup> 70 (IH 70)  
22 (D50: 215.00  $\mu$ m) was obtained from MEGGLE Group (Wasserburg, Germany) and used as a  
23 carrier. Magnesium stearate (MgSt) (D50: 6.92  $\mu$ m) was applied as a surface modifier (Sigma-  
24 Aldrich, Budapest, Hungary) of the carrier [34]. Sodium stearate (NaSt) (Alfa Aesar, Heysham,

1 United Kingdom) was used for a surface modifier of the co-spray dried particles [35]. Both of  
2 them are frequently applied moisture protective agents [36,37].

## 3 **2.2. Methods**

### 4 *2.2.1. Preparation of the samples*

5 For the stability test, we again produced the samples which had been examined in our previous  
6 work [18]. We prepared carrier-based, carrier-free, and novel combined formulated DPI  
7 systems. Table 1. contains the w/w % compositions of these samples. The carrier-based  
8 formulation ( $\mu$ CIP+IH70) – as a reference [38] – was prepared with mixing in 1:10 [39] mass  
9 ratio of the drug and carrier by turbula blending (Turbula System Schatz; Willy A. Bachofen  
10 AG Maschinenfabrik, Basel, Switzerland) for half an hour at 60 rpm [36]. The **carrier-free**  
11 formulation (CIP\_0.5NaSt\_spd) was produced from a solution with co-spray-drying of CIP and  
12 NaSt. Firstly, we made a 1.5 w/v % aqueous solution using CIP and the alcoholic solution  
13 containing 0.0175 w/v % NaSt at 30 °C. Then the two solutions were mixed in the 7: 3 ratio.  
14 Büchi B-191 apparatus (Mini Spray Dryer, Büchi, Switzerland) was applied for the co-spray-  
15 drying procedure with the following parameters: inlet heating temperature, 130 °C, outlet  
16 heating temperature, 78 °C, aspirator capacity, 75 %, pressured air flow, 600 L/min, feed pump  
17 rate, 5 %. So the solid formulation contained 99.5 w/w % of CIP and 0.5 w/w % of NaSt. The  
18 novel combined formulated sample (CIP\_0.5NaSt\_spd+IH70\_MgSt) combined the two above-  
19 mentioned preparation methods supplemented with carrier surface treatment. The surface  
20 modification of IH 70 carrier was made by 2.0 w/w % of MgSt (according to the literature  
21 background and the applied marketed concentration [40,41] ) with turbula mixing for 4 h [34].  
22 Then we prepared co-spray-dried particles as described in the carrier-free section and these  
23 particles were blended with a surface smoothed carrier in the 1:10 mass ratio with a turbula  
24 mixer at 60 rpm for 30 min.

1 **Table 1. Composition of the DPI formulations containing the applied concentration of**  
2 **excipients.**

3 *2.2.2. Investigation of the stability of samples*

4 Stability tests were performed in Binder KBF 240 (Binder GmbH Tuttlingen, Germany)  
5 equipment, with a constant-climate chamber. An electronically controlled APT.line™ line  
6 preheating chamber and refrigerating system ensured temperature accuracy and reproducibility  
7 of the results in the temperature range between 10 and 70 °C and the RH (Relative Humidity)  
8 range between 10 and 80 %. The stability test was performed at  $25 \pm 2$  °C with  $50 \pm 5$  % RH  
9 (room conditions). Samples were stored in hard gelatine capsules (size 3) (Capsugel, Germany)  
10 in open containers; the duration of storage was 1 month. Sampling was carried out after 0 and  
11 10 days, and 1 month.

12 *2.2.3. X-ray powder diffraction (XRPD)*

13 XRPD was implemented in order to determine the crystalline form of the produced DPI  
14 formulations. The powder samples were loaded in contact with a plane quartz glass sample slide  
15 with an etched square, and measured with a slit detector Cu K  $\lambda_1$  radiation ( $\lambda = 1.5406$  Å) source.  
16 Settings were as follows: the samples were scanned at 40 kV and 40 mA and the angular range  
17 was  $3^\circ$ – $40^\circ$   $2\theta$ , at a step time of 0.1 s/step and a step size of  $0.01^\circ$ .

18 *2.2.4. FT-IR analysis*

19 An FT-IR apparatus was used before and after storage for the study of the interaction between  
20 the components and test the chemical stability of the materials. FT-IR spectra were recorded  
21 with a Bio-Rad Digilab Division FTS- 65A/896 FTIR spectrometer (Bio-Rad Digilab Division  
22 FTS-65A/869, Philadelphia, PA, United States) between 4000 and  $400\text{ cm}^{-1}$ , at an optical  
23 resolution of  $4\text{ cm}^{-1}$ . Thermo Scientific GRAMS/AI Suite software (Thermo Fisher Scientific  
24 Inc., Waltham, United States) was used for the spectral analysis. The sample, with a CIP content

1 of 0.5 mg, was mixed with 150 mg of dry KBr in an agate mortar, and the mixture was then  
2 compressed into a disc at 10 t. Each disc was scanned 128 times at a resolution of  $2\text{ cm}^{-1}$  over  
3 the wavenumber region  $4000\text{-}400\text{ cm}^{-1}$ .

#### 4 2.2.5. *Thermogravimetry (TG)*

5 Residual solvent content was investigated by TG-DTA with a Mettler Toledo TG 821e thermal  
6 analysis system with the STAR<sup>e</sup> thermal analysis program V9.1 (Mettler Inc., Schwerzenbach,  
7 Switzerland) under a constant flow of dry nitrogen gas flow of  $100\text{ mL min}^{-1}$ . Aluminium pans  
8 were applied for the samples and the reference. Scans were recorded at a constant heating rate  
9 ( $10\text{ °C min}^{-1}$ ) up to  $350\text{ °C}$ . The TG-DTA oven was pre-equilibrated at room temperature and  
10 each sample (ranging between 12 and 20 mg) was weighed as fast as possible in order to  
11 minimize moisture uptake or release from the sample. The mass losses were recorded, and the  
12 moisture contents [% wet basis] were evaluated from the normalized scans, the actual mass is  
13 divided by the initial mass. The loss of water basically occurred between 5 and  $110\text{ °C}$ , and the  
14 higher temperature was used for the determination of bound water.

#### 15 2.2.6. *Interparticle interactions*

16 Contact angle ( $\Theta$ ) was determined by using a Dataphysics OCA 20 apparatus (Dataphysics Inc.  
17 GmbH, Germany), from which we could count some of the correlations (see below). The  
18 pastilles were pressed from 0.10 g of the samples with 1 ton compression force (Perkin Elmer  
19 hydraulic press, Waltham, USA). Six pastilles were made of each sample. Of this, three were  
20 dripped with distilled water (as a polar liquid) and the other three pastilles were dripped with  
21 diiodomethane (as dispersion liquid). Thus, we obtained the contact angle of the two different  
22 fluids by three parallel tests per sample. At the same time as the dropping, we made a recording  
23 by using the device in 1-25 seconds time interval, so it was possible to detect and determine the  
24 change of the contact angle. The surface free energy ( $\gamma_s$ ) of the samples was calculated based



1 on the Wu-equation. This energy consists of two parts: a disperse part ( $\gamma_s^d$ ) and a polar part ( $\gamma_s^p$ )  
 2 ), thereby ( $\gamma_s = \gamma_s^d + \gamma_s^p$ ). The surface tension of the liquids is known in literature  
 3 ( $\gamma_l = \gamma_l^d + \gamma_l^p$ ): distilled water  $\gamma^p=50.2$  mN/m,  $\gamma^d=22.6$  mN/m and diiodomethane  $\gamma^p=1.8$   
 4 mN/m,  $\gamma^d=49$  mN/m [42]. In the Wu-equation, therefore, there are only two unknowns: the  
 5 disperse ( $\gamma_s^d$ ) and the polar component ( $\gamma_s^p$ ) of the solids tested, which can already be expressed.  
 6 The Wu-equation is the following [43]:

$$(1 + \cos \Theta)\gamma_l = \frac{4(\gamma_s^d \gamma_l^d)}{\gamma_s^d + \gamma_l^d} + \frac{4(\gamma_s^p \gamma_l^p)}{\gamma_s^p + \gamma_l^p}$$

7  
 8 where  $\Theta$  = contact angle;  $\gamma$  = surface free energy; s = solid phase; l = liquid phase; d =  
 9 dispersion component; p = polar component

10 Cohesion work ( $W_c$ ) corresponds to twice the surface free energy [44]:

$$W_c = 2 * \gamma_s$$

11  
 12 The adhesion work ( $W_{adh}$ ) that can be interpreted between the two different materials  
 13 (represented by numbers 1 and 2) can be determined from the dispersion ( $\gamma_s^d$ ) and polar  
 14 component ( $\gamma_s^p$ ) values calculated for the material in the present formula  $\gamma^d$  and  $\gamma^p$ , and it  
 15 equals [44]:

$$W_{adh} = 4 \left[ \frac{\gamma_1^d \gamma_2^d}{\gamma_1^d + \gamma_2^d} + \frac{\gamma_1^p \gamma_2^p}{\gamma_1^p + \gamma_2^p} \right]$$

16  
 17 Several models are known for the determination of adhesion force ( $F_{adh}$ ). In our present work  
 18 we used Derjaguin's approach, which is commonly used in pharmaceutical technology [43]:

$$F_{adh} = 2\pi \left( \frac{R_A R_B}{R_A + R_B} \right) W_{adh}$$

19

1 where  $R_A$  and  $R_B$  are the radius of the A and B particles, between which adhesive interactions  
2 were measured.  $R$  was defined as half of  $D$  [0.5], which was determined in the particle size  
3 analysis of the used raw materials.

4 The spreading coefficient ( $S_{12}$ ) shows the spreadability of one material (1) on the surface of the  
5 other material (2). Conversely, it can be calculated. It is used in two-component systems to  
6 characterize distribution. This coefficient is a dimensionless number. Spreading is favorable if  
7 the result is a positive value, and the higher the number. In this case, the spreading of the drug  
8 particles can be characterized on the surface of the carrier. The coefficient or reverse case can  
9 be calculated using the following equations [43,44]:

$$10 \quad S_{12} = 4 \left[ \frac{\gamma_1^d \gamma_2^d}{\gamma_1^d + \gamma_2^d} + \frac{\gamma_1^p \gamma_2^p}{\gamma_1^p + \gamma_2^p} - \frac{\gamma_1}{2} \right]$$

$$11 \quad S_{21} = 4 \left[ \frac{\gamma_1^d \gamma_2^d}{\gamma_1^d + \gamma_2^d} + \frac{\gamma_1^p \gamma_2^p}{\gamma_1^p + \gamma_2^p} - \frac{\gamma_2}{2} \right]$$

12 where  $\gamma^d$  is the disperse part of surface free energy and  $\gamma^p$  is the polar part of surface free energy  
13 and  $\gamma$  is the total surface free energy of the components whose is spread on the other component.

#### 14 2.2.7. Particle size analysis

15 The particle size distribution of the used active ingredients, excipients, and the formulations  
16 before and after storage from the dry dispersion unit were also measured by laser light scattering  
17 (Malvern Mastersizer Scirocco 2000, Malvern Instruments Ltd., Worcestershire, UK).  
18 Approximately 0.5 g of composition was loaded into a feeder tray. In the dry analysis method,  
19 the air was used as the dispersion agent for the sample particles. The dispersion air pressure  
20 was adjusted to 2.0 bars in order to determine whether particle attrition had occurred. At least

1 three repeated measurements were made on each sample, and the mean value was calculated.  
2 Particle size distribution was characterized by the D[0.1], D[0.5], and D[0.9] values.

### 3 2.2.8. *Scanning electron microscopy (SEM)*

4 The morphology of the samples was investigated by scanning electron microscopy – SEM –  
5 (Hitachi S4700, Hitachi Scientific Ltd., Tokyo, Japan). The samples were coated with an  
6 electrically conductive coating (Bio-Rad SC 502, VG Microtech, Uckfield, UK). The air  
7 pressure was 1.3-13.0 MPa. In brief, the samples were sputter coated with gold–palladium (90  
8 seconds) under an argon atmosphere applying a gold sputter module in a high vacuum  
9 evaporator and the samples were studied using SEM set at 10-15 kV.

### 10 2.2.9. *Aerodynamic assessment with the Andersen Cascade Impactor Model*

11 The *in vitro* aerodynamic properties of the formulations were tested with the Andersen Cascade  
12 Impactor (ACI) (Copley Scientific Ltd., Nottingham, UK), which is a most commonly used to  
13 characterize the aerosolization performance of the inhaled DPIs. This corresponds to the United  
14 States Pharmacopeia and Ph. Eur. 2.9.18 requirements [26,45]. The vacuum pump (High-  
15 capacity Pump Model HCP5, Critical Flow Controller Model TPK, Copley Scientific Ltd.,  
16 Nottingham, UK) provided 28.3 L/min flow rate and a corresponding ACI assembly was  
17 applied to that flow. The actual flow rate through the impactor was detected with the mass flow  
18 meter (Flow Meter Model DFM 2000, Copley Scientific Ltd., Nottingham, UK). Before each  
19 test, to prevent particle bounce the ACI collection plates were coated with a surfactant (Span  
20 80 + cyclohexane solution; 1 + 99 w/w %), so repeated inhalation into the cascade impactor  
21 was possible. In our experiments, the samples were measured in a hard gelatin capsule  
22 (transparent, size 3, Capsugel, Germany). The drug content of the formulations was detected  
23 with an UV/Vis spectrophotometer (ATI-UNICAM UV/VIS Spectrophotometer, Cambridge,  
24 UK). The amounts charged into the capsules were determined so that the CIP content per sample

1 was 10 mg [12]. This mass corresponds to the tenth of the CIP oral dose [27]. During our testing,  
2 Breezhaler<sup>®</sup> (Novartis) inhaler was used. The filled capsule was placed in this inhaler and then  
3 with the help of the needles of the appliance the capsule was punched with a definite movement.  
4 Because of the big amount of carrier lactose, in the cases of carrier-based and novel  
5 formulations, to apply the same amount of CIP (10 mg), we used 2 capsules per one dose  
6 application. The DPI device, the mouthpiece, the induction port, the eight plates of the impactor,  
7 and the filter were washed with distilled water and the CIP concentration was quantified with  
8 an UV/Vis spectrophotometer (ATI-UNICAM UV/VIS Spectrophotometer, Cambridge, UK)  
9 at 276 nm. Knowing the amount of the active ingredient in the device and in the parts of the  
10 impactor, the emitted fraction (EF), fine particle fraction (FPF) and mass median aerodynamic  
11 diameter (MMAD) were determined. FPF expresses the fraction of particles having an  
12 aerodynamic diameter less than 5 micron, these particles are likely to be deposited in the lungs.  
13 However, more and more publications express the percentage of particles below 3 microns as  
14 they are most likely to reach the deep lung [46,47]. MMAD is defined as the diameter of the  
15 particles deposited in the impactor for which 50% w/w of particles have a lower diameter and  
16 50% w/w have a higher diameter [48]. EF was expressed as the percentage of the drug found in  
17 the ACI (except the drug found in the capsules and device). Only the drug concentration was  
18 determined by analytical method. Therefore we can use this data by the calculation of emitted  
19 fraction.

#### 20 *2.2.10. In silico characterization*

21 For the estimation of the amount of drug depositing in different anatomical regions of the  
22 airways (upper airways, lungs), the most up-to-date version of the Stochastic Lung Model  
23 (SLM) of Koblinger and Hofmann (1990) [49] was applied. Indeed, the impactor measurements  
24 can demonstrate the repeatability of formulation batches and reveal the aerodynamic properties  
25 (size, size distribution) of the sample. However, these data can be used as predictors of airway

1 deposition as well, with the mentioning that impactor measurements cannot provide exact  
2 airway deposition values like the scintigraphic studies. However, computer models validated  
3 against scintigraphic measurements (like the one presented in this study) are able to estimate  
4 the deposited amount quite exactly. Deposition in the extrathoracic region was calculated based  
5 on the formulas derived by Cheng (2003) [50]. Particles which were not filtered out by the  
6 upper airways were tracked in stochastic tracheobronchial geometry. Airway lengths,  
7 diameters, bifurcation angles and gravity angles were selected from statistical distributions  
8 based on the morphometric database of Raabe et al. (1976) [51]. The architecture of the acinar  
9 airways relied on the data published by Haefeli-Bleuer and Weibel (1988) [52]. Inertial  
10 impaction and gravitational settling were considered as deposition mechanisms in both the  
11 bronchial and acinar parts of the airways. Particle size distributions determined by Andersen  
12 Cascade impactor as part of this work were used as inputs for the deposition simulations. In  
13 addition, the breathing parameters of a patient when inhaling through Breezhaler<sup>®</sup> were used as  
14 modeling inputs (inhaled air volume: 1.7 L, inhalation time: 3.2 s, breath-hold time after the  
15 inhalation: 5 s and 10 s, exhalation time: 3 s). The breathing parameters were adopted from the  
16 work of Colthorpe et al. (2015) and corresponded to a female patient with moderate COPD.  
17 The exact deposition values naturally depend on the disease type and degree of severity,  
18 however, the main conclusions of the present work would not be affected. The simulated high  
19 lung deposition values associated with the formulation would even increase for patients with  
20 less impaired lung function. These data correspond to the breathing parameter values measured  
21 by Colthorpe et al. (2013) [53]. This patient was selected because his/her inhalation parameter  
22 values yield an average flow rate value very close to 30 L/min, which was applied in the present  
23 impactor measurements.

#### 24 *2.2.11. Statistical analyses*

1 The statistical analyses were performed with the Social Science Statistics Online web page  
2 2019. For the stability assessment using t-test calculation at 0.05 significance level and one-  
3 tailed hypothesis (Social Science Statistics Online). All reported data are means  $\pm$  S.D of three  
4 parallel measurements (n=3).

5

### 6 **3. Results and discussion**

#### 7 **3.1. Structural characterization**

#### 8 **Figure 1. Structural investigation of the formulations by XRPD before and after storage**

9 XRPD makes it possible to track the structural changes of the DPI samples during storage,  
10 which can be analyzed if the XRPD patterns of CIP and of the used excipients are known.  
11 Specifically, the characteristic of the solid state form of the active ingredient particles could be  
12 very important, since the crystalline form or amorphous form could present results in  
13 morphological differences and influences the interparticle interactions, thus affecting the  
14 aerodynamic results. According to the XRPD diffractograms (Figure 1.A), we can determine  
15 the characteristic peaks of the starting materials. These are the following: 12.8, 16.8 and 20.0  
16 *2Theta degree* of IH 70; 8.23, 9.25, 19.22, 26.39 and 29.16 *2Theta degree* of CIP; 3.8, 5.5  
17 *2Theta degree* of MgSt and 4.0, 6.0 *2Theta degree* of NaSt. All of these materials are crystalline.  
18 We can conclude that the surface modification of IH 70 with 2 w/w% MgSt did not cause any  
19 change in the XRPD pattern, thus not causing any structural change either.

20 In the case of samples (Figure 1.B) it can be concluded that CIP could be found mainly in  
21 amorphous form in the CIP\_0.5NaSt\_spd, however the characteristic peaks of NaSt and CIP  
22 (with small intensity) could be found on the curve before storage, but after 1 month complete  
23 recrystallization is seen and the CIP XRPD pattern in the above figure is almost identical.  
24 However, based on the peaks at 8.23, 9.25 and 26.39 *2Theta degree*, we can make statements

1 about carrier-based formulations as well. Thus for  $\mu$ CIP+IH70 it can be established that the  
2 initial crystalline nature of the active ingredient particles remains, and there is no change. In the  
3 case of freshly prepared CIP\_0.5NaSt\_spd+IH70\_MgSt, the active ingredient particles were  
4 **mainly** amorphous similarly to CIP\_0.5NaSt\_spd, but after 1 month a substantial amount of  
5 crystal structure change is not apparent on the XRPD pattern, which indicates that  
6 CIP\_0.5NaSt\_spd+IH70\_MgSt has greater structural stability relative to the latter composition.  
7 **Therefore the crystalline peaks correspond to IH 70.**

8 According to the FT-IR analyses, the FT-IR spectra of the raw components and the prepared  
9 samples before and after storage **compared** with each other (Figures are not presented in the  
10 article). We concluded that no chemical decomposition was presumable.

### 11 **3.2. Thermogravimetry (TG)**

#### 12 **Table 2. Residual solvent content in samples.**

13 The determination of thermogravimetric residual solvent content for DPIs is of key importance  
14 in tracking the stability of samples. By increased residual solvent content decreased stability is  
15 presumable. An increase in this value may indicate a decrease in stability. Moisture sorption  
16 can cause the agglomeration of the particles; can modify interparticle interactions and influence  
17 drug dispersion; de-agglomeration, which affects the lung deposition results [54]. The  
18 percentages resulting from residual solvent content (Table 2.) from our measurements are  
19 realistic for DPIs [55]. We have found that the residual solvent content has increased after 1  
20 month for the  $\mu$ Cip +IH70 and CIP\_0.5NaSt\_spd formulations. For example, it provides an  
21 explanation for the recrystallization of the latter composition. In the case of the novel combined  
22 formulated DPI (CIP\_0.5NaSt\_spd+IH70\_MgSt) residual solvent content did not change, and  
23 it decreased slightly. The present of MgSt caused the moisture resistance of the composition  
24 and this phenomenon already described in the international literature [36] has been confirmed

1 by us. It has also been found that the moisture resistance of the DPI composition is improved  
2 by the use of MgSt as an excipient. The largest residual solvent content change was observed  
3 for the CIP\_0.5NaSt\_spd formulation, in contrast, there was no significant change in the novel  
4 combined formulated DPI (CIP\_0.5NaSt\_spd+IH70\_MgSt), which also contains  
5 CIP\_0.5NaSt\_spd.

### 6 **3.3. *Interparticle interactions***

#### 7 **Table 3. Cohesion, adhesion values and spreading coefficient of the formulations.**

8 Interparticle interactions have already been studied in our previous work [18]. Cohesive work  
9 ( $W_c$ ) in the carrier-free formulations (between the drug particles), furthermore, adhesive work  
10 ( $W_{adh}$ ) and force ( $F_{adh}$ ) in the carrier-based formulations (between drug and carrier particles)  
11 are correlated with the *in vitro* lung deposition results. The studies were performed after a period  
12 of 1 month storage, as shown in Table 3., the  $F_{adh}$  of  $\mu$ CIP+IH70 did not change, this means  
13 that the active ingredient particles continue to adhere strongly to the carrier, so a low FPF value  
14 is expected after 1 month, too. In the case of CIP\_0.5NaSt\_spd,  $W_c$  increased substantially,  
15 approaching the value of fully crystalline  $\mu$ CIP, resulting from recrystallization and residual  
16 solvent content growth that contribute to interparticle interaction change. As cohesion between  
17 the active ingredient particles is increased, they can aggregate more easily. For the novel  
18 combined formulated DPI (CIP\_0.5NaSt\_spd+IH70\_MgSt),  $F_{adh}$  did not increase greatly, still  
19 not reaching the value of adhesion of  $\mu$ CIP+IH70, and the spreading coefficient ( $S_{21}$ ) remained  
20 in the negative range left. The latter suggests that a vectored drug position can still be assumed  
21 on the surface of the carrier, it is not completely covered with it. All this - encountered with  
22 CIP\_0.5NaSt\_spd+IH70\_MgSt - can be explained by the structure testing and the residual  
23 solvent content experience. Thus, it is expected that the FPF value will be outstanding in the *in*  
24 *vitro* lung deposition assay after 1 month.



1 **3.4. Particle size analysis and scanning electron microscopy (SEM)**

2 **Table 4. Morphology and particle size distribution of the formulations during the**  
3 **storage.**

4 The study of particle size distribution and the morphology of the DPI samples also has great  
5 importance during storage. According to existing literature, it can be said that the range of 1-5  
6 microns is the optimal drug particle size for appropriate lung deposition. Particles greater than  
7 5 microns are deposited in the throat and trachea with great probability and most of the  
8 submicron particles are exhaled [56]. Furthermore, in terms of morphology, it can be stated that  
9 spherical particles produced by spray-drying have a low contact area; homogeneous particle  
10 size distribution and these result in a higher FPF than in the case of mechanically micronized  
11 drugs [57]. Table 4 shows the results of SEM and laser light scattering. We can conclude that  
12 the (average) diameters measured by Malvern and SEM are in correlation. We focused on the  
13 active ingredient particles on SEM. The average particle size of the drug particles remained in  
14 the range of 1-5 microns nevertheless, it increased for all formulations during the stability test,  
15 which can somewhat reduce the lung deposition results. In the case of the  $\mu$ CIP+IH70  
16 formulation, no aggregation or morphological changes can be observed after 1 month. After 1  
17 month, the CIP\_0.5NaSt\_spd formulation shows the recrystallization and aggregation of the  
18 particles, which is also indicated by XRPD; residual solvent content; cohesion results and the  
19 significantly increased D [0.9] value. In contrast, there is no significant morphological change  
20 which would refer to recrystallization; and there is no aggregation even in SEM images in terms  
21 of the CIP\_0.5NaSt\_spd+IH70\_MgSt formulation containing the spray-dried drug particles –  
22 of the same method as the sample mentioned above – on the surface modified carrier. We  
23 collected the D [0.5] values of the drug and the carrier by the carrier-based formulations using  
24 the bimodal distribution curves (see table below). However, D [0.1] and D [0.9] could be  
25 determined only for the formulations. We concluded that the size of CIP in  $\mu$ CIP+IH70 sample

1 changed from 4.92  $\mu\text{m}$  to 5.34  $\mu\text{m}$  and the size of IH70 changed from 180.03  $\mu\text{m}$  to 186.66  $\mu\text{m}$ .  
2 Furthermore, the size of CIP\_0.5NaSt\_spd in CIP\_0.5NaSt\_spd+IH70\_MgSt sample changed  
3 from 2.27  $\mu\text{m}$  to 2.57  $\mu\text{m}$  and the size of IH70\_MgSt changed from 171.12  $\mu\text{m}$  to 179.45  $\mu\text{m}$ .  
4 If we compare the change in D [0.5] size of CIP\_0.5NaSt\_spd and of CIP\_0.5NaSt\_spd in  
5 CIP\_0.5NaSt\_spd+IH70\_MgSt we can see that in the combined formulation the size changing  
6 was smaller than by the carrier-free sample. Therefore, in the case of the novel combined  
7 formulated formulations, high FPF values are still expected in terms of *in vitro* lung deposition.

### 8 **3.5. Aerodynamic assessment with the Andersen Cascade Impactor Model**

9 **Table 5. FPF value of microparticles before and after storage.**

10 **Table 6. EF and MMAD values of microparticles before and after storage.**

11 *In vitro* lung modeling with the Andersen Cascade Impactor results in FPF, MMAD and EF  
12 (Table 5., 6.) that have been defined in the Method section. The quantities of the samples were  
13 chosen after drug content determination, where the measured drug content was between 82 and  
14 93% compared to the theoretical drug content. We concluded that these values didn't change  
15 after the storage also. The lung deposition values (FPF) were based on the results of physical  
16 examinations (XRPD, residual solvent content, interparticle interactions, morphology and  
17 particle size). Thus, after 1 month of storage, the novel combined formulated DPI  
18 (CIP\_0.5NaSt\_spd+IH70\_MgSt) had the best FPF results, outstandingly high FPF <3  $\mu\text{m}$ ,  
19 which indicates a high deep-lung deposition (approximately three times the FPF <3  $\mu\text{m}$  value  
20 of  $\mu\text{CIP+IH70}$  and double of CIP\_0.5NaSt\_spd). This is due to the fact that there is no  
21 significant change in the structure and residual solvent content of this composition (in fact, the  
22 latter changed favorably), thus the adhesion values did not increase substantially and its  
23 morphology did not change the active ingredient particles. All this leads to a reduction in the  
24 lung deposition result compared to the freshly made formulation. In contrast, CIP\_0.5NaSt\_spd

1 (it should be noted again that there is such an active ingredient particle in the novel combined  
2 formulated formulation, and also that these particles passed down into the lung in both  
3 formulations, but scattered from the carrier at the CIP\_0.5NaSt\_spd+IH70\_MgSt)  
4 recrystallized, the residual solvent content increased and these led to an increase in cohesion  
5 work, its morphology became disadvantageous and aggregated. Thus, FPF <3  $\mu\text{m}$  and FPF <5  
6  $\mu\text{m}$  values almost fell by half after 1 month of storage. For  $\mu\text{CIP} + \text{IH70}$  (reference sample), it  
7 has been found that the FPF <5  $\mu\text{m}$  value remained about 20%, which is typical for most of the  
8 marketed formulations [26]. The decrease in FPF, which is characteristic of all formulations,  
9 can be correlated with the established average particle size increase of CIP\_0.5NaSt\_spd in the  
10 formulation. Concerning MMAD, we found that the MMAD value is inversely proportional to  
11 the FPF values and only CIP\_0.5NaSt\_spd+IH70\_MgSt indicates that the particle size  
12 measured with laser light scattering and the MMAD calculated with *in vitro* pulmonary  
13 modeling are also around the ideal 1-5 micron range. The EF for the formulations containing  
14 the carrier ( $\mu\text{CIP} + \text{IH70}$  and CIP\_0.5NaSt\_spd+IH70\_MgSt) was very high and was not  
15 considerably altered during storage, however, this value of the carrier-free formulation  
16 (CIP\_0.5NaSt\_spd) increased, presumably due to structural change (hence the morphology  
17 change), so the interparticle interactions between the capsule wall and the particles were  
18 modified favourably.

### 19 **3.6. *In silico* assessment of particle deposition**

20 **Figure 2. *In silico* lung modeling results of the novel combined formulated DPI, SD <  $\pm$**   
21 **3% (ET: extrathoracic airways, LUNG: bronchial and acinar parts, EXH: exhalation**  
22 **fraction).**

23 The *in vitro* lung modeling we used is entirely suitable for comparing the aerodynamic  
24 properties of the DPI formulations. At the same time, the results from the measurements with  
25 Andersen Cascade Impactor are well complemented with the *in silico* lung modeling, which

1 takes into account parameters other than the above-mentioned results. As the *in vitro*  
2 investigations revealed, the novel formulation is characterized by very high and nearly emitted  
3 fraction value which remained nearly constant over time (Table 5). The fine particle fractions  
4 remained also high after storage (Table 6). The MMAD values remained in the favourable  
5 aerodynamic range regarding deposition (especially the MMAD value after 10 days of storage).  
6 All these characteristics predicted high lung deposition values not only of the fresh sample, but  
7 also after storage. All these predictions were confirmed by the *in silico* results depicted in Figure  
8 2. In addition, the validated numerical models simulate the *in vivo* conditions using real-  
9 spirometric data, so they give a more realistic picture of the behavior patterns during inhalation  
10 as they take real clinical data into consideration. We can type in individualized data based on  
11 age; sex; type and severity of lung disease. It should be noted, however, that in the above-  
12 mentioned two pulmonary models, the expressed lung deposition values have different  
13 interpretations (this is the explanation for the different percentages of FPF values by *in vitro*  
14 and LUNG values by *in silico*), but it is absolutely possible to compare the tendencies of the  
15 formulations and the two methods support each other. The *in silico* measurements were carried  
16 out in Section 2.2.9. In our previous work, the *in vitro* and *in silico* results of fresh samples  
17 ( $\mu$ CIP + IH70; CIP\_0.5NaSt\_spd; CIP\_0.5NaSt\_spd + IH70\_MgSt) showed the same tendency  
18 [18]. The *in silico* results of the formulation with the best *in-vitro* pulmonary deposition values  
19 (CIP\_0.5NaSt\_spd + IH70\_MgSt) after 10 days and 1 month of storage is shown in Figure 2  
20 with 5 s and 10 s as breath-hold time. The figure reveals that, as predicted by the *in vitro*  
21 characterization, this formulation yielded high simulated lung deposition fraction values. At the  
22 same time, the extrathoracic dose fraction remained below 30% after storage (even decreased  
23 by storage). This is a significant improvement compared to the other two formulations. The  
24 freshly produced CIP\_0.5NaSt\_spd (carrier-free) had approximately 40 %, upper airway  
25 deposition, while  $\mu$ CIP + IH70 (carrier-based) yielded a 50 % value [18]. The exhaled dose

1 fraction was approximately 20% and decreased by the increase of breath-hold time, while the  
2 extrathoracic dose fraction proved to be insensitive to the length of breath-hold. Lung  
3 deposition was higher for longer breath-hold indicating that the optimization of the inhalation  
4 technique can contribute to further improving the pulmonary deposition of the novel combined  
5 formulated DPI and to reducing the exhaled amount.

## 6 **Conclusion**

7 Stability tests were carried out on carrier-based, carrier-free, and novel combined formulated  
8 DPI sample (CIP\_0.5NaSt\_spd + IH70\_MgSt), containing antibiotic. After the storage, the  
9 novel combined formulation presented advantageous aerodynamic results thanks to the  
10 technological steps and the compositions. This sample has the most beneficial MMAD (2,5  $\mu\text{m}$ )  
11 and best FPF ( $<5 \mu\text{m}$ ; 50 %) results after 1 month, followed by the carrier-free, and the worst  
12 results are shown by the carrier-based formulations (as concluded by, for example, high residual  
13 solvent content, high  $W_{\text{adh}}$  and aerodynamically unfavourable morphology). From the results  
14 of the physicochemical examinations, we can conclude that in the case of the novel combined  
15 formulated sample (CIP\_0.5NaSt\_spd + IH70\_MgSt), an appreciable amount of crystal  
16 structure change is not apparent on the XRPD pattern, the residual solvent content was slight  
17 due to the MgSt and NaSt content. As regards interparticle interactions, it can be stated that the  
18 adhesion force of  $\mu\text{CIP} + \text{IH70}$  has remained high during the stability test, while in the case of  
19 CIP\_0.5NaSt\_spd, cohesion work has increased considerably, indicating that this formulation  
20 is easier to aggregate, which is also supported by electron microscopic images, and the  
21 recrystallization on the images could be seen. Based on these results, CIP\_0.5NaSt\_spd +  
22 IH70\_MgSt introduced suitable stability, therefore required physicochemical properties  
23 compare with the carrier-free formulation (where the preparation of the contained drug particles  
24 was the same). However, after 1 month of storage, by the EF values, a good percentage of all  
25 the three formulations was observed, The novel combined formulated sample with the best *in*

1 *vitro* lung deposition results was chosen for *in silico* lung modeling, and it was in correlation  
2 with the *in vitro* aerodynamic results. It should be emphasized that this sample had an  
3 extrathoracic dose fraction value below 30 % even after one month, while the freshly produced  
4 samples from the other two samples also had worse results. Finally, it can be stated that a novel  
5 combined formulated DPI formulation with favourable physicochemical characters after 1  
6 month storage, resulted improved *in vitro-in silico* aerodynamic properties which could be the  
7 reason to get stable formulation for the further development of DPIs.

## 8 **Declaration of interest**

9 The authors report no conflicts of interest in this work.

## 10 **Acknowledgment**

11 This project was supported by the UNKP-18-3 New National Excellence Program of the  
12 Ministry of Human Capacities and by EFOP-3.6.2-16-2017-00006 "LIVE LONGER -  
13 Development of Modern Medical Diagnostic Procedures and Therapies in a Translational  
14 Approach: from a laboratory to a patient bed" project.

15

## 1   **References**

- 2   [1]   Cystic fibrosis: Symptoms, causes, and management [Internet]. Med. News Today.  
3       2018 [cited 2018 Jul 2]. Available from:  
4       <https://www.medicalnewstoday.com/articles/147960.php>.
- 5   [2]   Accurso FJ. 89 - Cystic Fibrosis. In: Goldman L, Schafer AI, editors. Goldmans Cecil  
6       Med. Twenty Fourth Ed. [Internet]. Philadelphia: W.B. Saunders; 2012 [cited 2018 Jul  
7       2]. p. 544–548. Available from:  
8       <http://www.sciencedirect.com/science/article/pii/B9781437716047000890>.
- 9   [3]   Montgomery ST, Mall MA, Kicic A, et al. Hypoxia and sterile inflammation in cystic  
10      fibrosis airways: mechanisms and potential therapies. *Eur. Respir. J.* 2017;49:1600903.
- 11   [4]   Shamsuddin AKM, Quinton PM. Native small airways secrete bicarbonate. *Am. J.*  
12      *Respir. Cell Mol. Biol.* 2014;50:796–804.
- 13   [5]   Vallières E, Elborn JS. Cystic fibrosis gene mutations: evaluation and assessment of  
14      disease severity [Internet]. *Adv. Genomics Genet.* 2014 [cited 2018 Jul 2]. Available  
15      from: [https://www.dovepress.com/cystic-fibrosis-gene-mutations-evaluation-and-](https://www.dovepress.com/cystic-fibrosis-gene-mutations-evaluation-and-assessment-of-disease-se-peer-reviewed-fulltext-article-AGG)  
16      [assessment-of-disease-se-peer-reviewed-fulltext-article-AGG](https://www.dovepress.com/cystic-fibrosis-gene-mutations-evaluation-and-assessment-of-disease-se-peer-reviewed-fulltext-article-AGG).
- 17   [6]   FAARC MM RRT. PulmoSal™ 7% (pH+) Bio-Balanced™ Hypertonic Saline  
18      [Internet]. [cited 2018 Jul 2]. Available from: <https://westmedinc.com/pulmosal/>.
- 19   [7]   Goss CH, Burns JL. Exacerbations in cystic fibrosis · 1: Epidemiology and  
20      pathogenesis. *Thorax.* 2007;62:360–367.
- 21   [8]   Rogers DF. Mucociliary dysfunction in COPD: effect of current pharmacotherapeutic  
22      options. *Pulm. Pharmacol. Ther.* 2005;18:1–8.
- 23   [9]   Strong P, Ito K, Murray J, et al. Current approaches to the discovery of novel inhaled  
24      medicines. *Drug Discov. Today.* 2018;23:1705–1717.
- 25   [10]   Donald PR, McIlleron H. Chapter 59 - Antituberculosis drugs. In: Schaaf HS, Zumla  
26      AI, Grange JM, et al., editors. *Tuberculosis* [Internet]. Edinburgh: W.B. Saunders; 2009  
27      [cited 2018 Jul 5]. p. 608–617. Available from:  
28      <http://www.sciencedirect.com/science/article/pii/B9781416039884000597>.
- 29   [11]   Stockmann C, Sherwin CMT, Zobel JT, et al. Optimization of anti- pseudomonal  
30      antibiotics for cystic fibrosis pulmonary exacerbations: III. fluoroquinolones. *Pediatr.*  
31      *Pulmonol.* 2012;48:211–220.
- 32   [12]   Karimi K, Pallagi E, Szabó-Révész P, et al. Development of a microparticle-based dry  
33      powder inhalation formulation of ciprofloxacin hydrochloride applying the quality by  
34      design approach. *Drug Des. Devel. Ther.* 2016;10:3331–3343.
- 35   [13]   Denis O, Rodriguez-Villalobos H, Struelens MJ. Chapter 3 - The problem of resistance.  
36      In: Finch RG, Greenwood D, Norrby SR, et al., editors. *Antibiot. Chemother.* Ninth Ed.  
37      [Internet]. London: Saunders; 2010 [cited 2018 Jul 5]. p. 24–48. Available from:  
38      <http://www.sciencedirect.com/science/article/pii/B9780702040641000038>.

- 1 [14] Bosso JA. Use of ciprofloxacin in cystic fibrosis patients. *Am. J. Med.* 1989;87:S123–  
2 S127.
- 3 [15] W. S. Yapa S, Li J, Patel K, et al. Pulmonary and Systemic Pharmacokinetics of  
4 Inhaled and Intravenous Colistin Methanesulfonate in Cystic Fibrosis Patients:  
5 Targeting Advantage of Inhalational Administration. *Antimicrob. Agents Chemother.*  
6 2014;58:2570–2579.
- 7 [16] Pomázi A, Szabó-Révész P, Ambrus R. Pulmonal administration, aspects of DPI  
8 formulation. *Gyógyszerészet.* 2009;53:397–404.
- 9 [17] Pomázi A, Chvatal A, Ambrus R, et al. Potential formulation methods and  
10 pharmaceutical investigations of Dry Powder Inhalers. *Gyógyszerészet.* 2014;58:131–  
11 139.
- 12 [18] Ambrus R, Benke E, Farkas Á, et al. Novel dry powder inhaler formulation containing  
13 antibiotic using combined technology to improve aerodynamic properties. *Eur. J.*  
14 *Pharm. Sci.* 2018;123:20–27.
- 15 [19] Muralidharan P, Hayes D, Mansour HM. Dry powder inhalers in COPD, lung  
16 inflammation and pulmonary infections. *Expert Opin. Drug Deliv.* 2015;12:947–962.
- 17 [20] Varshosaz J, Taymouri S, Hamishehkar H, et al. Development of dry powder inhaler  
18 containing tadalafil-loaded PLGA nanoparticles. *Res. Pharm. Sci.* 2017;12:222–232.
- 19 [21] Yadav N, Lohani A. Dry Powder Inhalers: A Review. *Indo Glob. J. Pharm. Sci.*  
20 2013;3:142–155.
- 21 [22] Hooton JC, Jones MD, Harris H, et al. The influence of crystal habit on the prediction  
22 of dry powder inhalation formulation performance using the cohesive-adhesive force  
23 balance approach. *Drug Dev. Ind. Pharm.* 2008;34:974–983.
- 24 [23] Patil S, Mahadik A, Nalawade P, et al. Crystal engineering of lactose using electrospray  
25 technology: carrier for pulmonary drug delivery. *Drug Dev. Ind. Pharm.* 2017;43:2085–  
26 2091.
- 27 [24] Benke E, Szabó-Révész P, Hopp B, et al. Characterization and development  
28 opportunities of carrier-based dry powder inhaler systems. *Acta Pharm. Hung.*  
29 2017;87:59–68.
- 30 [25] Demoly P, Hagedoorn P, de Boer AH, et al. The clinical relevance of dry powder  
31 inhaler performance for drug delivery. *Respir. Med.* 2014;108:1195–1203.
- 32 [26] Chvatal A, Farkas Á, Balásházy I, et al. Aerodynamic properties and in silico  
33 deposition of meloxicam potassium incorporated in a carrier-free DPI pulmonary  
34 system. *Int. J. Pharm.* 2017;520:70–78.
- 35 [27] Benke E, Szabó-Révész P, Ambrus R. Development of ciprofloxacin hydrochloride  
36 containing dry powder inhalation system with an innovative technology. *Acta Pharm.*  
37 *Hung.* 2017;87:49–58.



- 1 [28] Karimi K, Katona G, Csóka I, et al. Physicochemical stability and aerosolization  
2 performance of dry powder inhalation system containing ciprofloxacin hydrochloride.  
3 *J. Pharm. Biomed. Anal.* 2018;148:73–79.
- 4 [29] Shetty N, Zeng L, Mangal S, et al. Effects of Moisture-Induced Crystallization on the  
5 Aerosol Performance of Spray Dried Amorphous Ciprofloxacin Powder Formulations.  
6 *Pharm. Res.* [Internet]. 2018 [cited 2018 Apr 12];35. Available from:  
7 <http://link.springer.com/10.1007/s11095-017-2281-5>.
- 8 [30] Akdag Cayli Y, Sahin S, Buttini F, et al. Dry powders for the inhalation of  
9 ciprofloxacin or levofloxacin combined with a mucolytic agent for cystic fibrosis  
10 patients. *Drug Dev. Ind. Pharm.* 2017;43:1378–1389.
- 11 [31] Adi H, Young PM, Chan H-K, et al. Cospray Dried Antibiotics for Dry Powder Lung  
12 Delivery. *J. Pharm. Sci.* 2008;97:3356–3366.
- 13 [32] Elborn JS. Ciprofloxacin dry powder inhaler in cystic fibrosis. *BMJ Open Respir. Res.*  
14 2016;3:1–2.
- 15 [33] McShane PJ, Weers JG, Tarara TE, et al. Ciprofloxacin Dry Powder for Inhalation  
16 (ciprofloxacin DPI): Technical design and features of an efficient drug–device  
17 combination. *Pulm. Pharmacol. Ther.* 2018;50:72–79.
- 18 [34] Cocconi D, Dagli Alberi M, Busca A, et al. Use of magnesium stearate in dry powder  
19 formulations for inhalation [Internet]. 2012 [cited 2018 Apr 11]. Available from:  
20 <https://patents.google.com/patent/US20120082727A1/en>.
- 21 [35] Parlati C, Colombo P, Buttini F, et al. Pulmonary Spray Dried Powders of Tobramycin  
22 Containing Sodium Stearate to Improve Aerosolization Efficiency. *Pharm. Res.*  
23 2009;26:1084–1092.
- 24 [36] Plastira M. The influence of Magnesium Stearate and carrier surface on the deposition  
25 performace of carrier based Dry Powder Inhaler formulations. 2008.
- 26 [37] Zhu B, Haghı M, Nguyen A, et al. Delivery of theophylline as dry powder for  
27 inhalation. *Asian J. Pharm. Sci.* 2015;10:520–527.
- 28 [38] Hamishehkar H, Rahimpour Y, Javadzadeh Y. The Role of Carrier in Dry Powder  
29 Inhaler. In: Sezer AD, editor. *Recent Adv. Nov. Drug Carr. Syst.* [Internet]. InTech;  
30 2012 [cited 2019 Mar 21]. Available from: [http://www.intechopen.com/books/recent-](http://www.intechopen.com/books/recent-advances-in-novel-drug-carrier-systems/the-role-of-carrier-in-dry-powder-inhaler)  
31 [advances-in-novel-drug-carrier-systems/the-role-of-carrier-in-dry-powder-inhaler](http://www.intechopen.com/books/recent-advances-in-novel-drug-carrier-systems/the-role-of-carrier-in-dry-powder-inhaler).
- 32 [39] Buttini F, Cuoghi E, Miozzi M, et al. Insulin spray-dried powder and smoothed lactose:  
33 a new formulation strategy for nasal and pulmonary delivery [Internet]. ResearchGate.  
34 2012 [cited 2018 Apr 11]. Available from:  
35 [https://www.researchgate.net/publication/284045495\\_Insulin\\_spray-](https://www.researchgate.net/publication/284045495_Insulin_spray-dried_powder_and_smoothed_lactose_a_new_formulation_strategy_for_nasal_and_pulmonary_delivery)  
36 [dried\\_powder\\_and\\_smoothed\\_lactose\\_a\\_new\\_formulation\\_strategy\\_for\\_nasal\\_and\\_pul-](https://www.researchgate.net/publication/284045495_Insulin_spray-dried_powder_and_smoothed_lactose_a_new_formulation_strategy_for_nasal_and_pulmonary_delivery)  
37 [monary\\_delivery](https://www.researchgate.net/publication/284045495_Insulin_spray-dried_powder_and_smoothed_lactose_a_new_formulation_strategy_for_nasal_and_pulmonary_delivery).
- 38 [40] Lau M, Young PM, Traini D. Co-milled API-lactose systems for inhalation therapy:  
39 impact of magnesium stearate on physico-chemical stability and aerosolization  
40 performance. *Drug Dev. Ind. Pharm.* 2017;43:980–988.

- 1 [41] Hazare S, Menon M. Improvement of Inhalation Profile of DPI Formulations by  
2 Carrier Treatment with Magnesium Stearate. *Indian J. Pharm. Sci.* 2009;71:725–727.
- 3 [42] Schuster JM, Schvezov CE, Rosenberger MR. Analysis of the Results of Surface Free  
4 Energy Measurement of Ti6Al4V by Different Methods. *Procedia Mater. Sci.*  
5 2015;8:732–741.
- 6 [43] Farkas B, Révész P. *Kristályosítástól a tablettázásig.* Universitas Szeged; 2007.
- 7 [44] Tüske Z. Influence of the surface free energy on the parameters of pellets. 2005.
- 8 [45] Brochures - Copley Scientific [Internet]. 2015 [cited 2018 Aug 23]. Available from:  
9 <http://www.copleyscientific.com/downloads/brochures>.
- 10 [46] Benke E, Farkas Á, Balásházy I, et al. The actuality of devices for the delivery of dry  
11 powder inhalation, formulations and modern assemblies I. *Gyógyszerészet/Pharmacy.*  
12 2018;62:131–139.
- 13 [47] Simon A, Amaro MI, Cabral LM, et al. Development of a novel dry powder inhalation  
14 formulation for the delivery of rivastigmine hydrogen tartrate. *Int. J. Pharm.*  
15 2016;501:124–138.
- 16 [48] Parlati C. Respirable microparticles of aminoglycoside antibiotics for pulmonary  
17 administration. 2008.
- 18 [49] Koblinger L, Hofmann W. Monte Carlo modeling of aerosol deposition in human  
19 lungs. Part I: Simulation of particle transport in a stochastic lung structure. *J. Aerosol*  
20 *Sci.* 1990;21:661–674.
- 21 [50] Cheng YS. Aerosol deposition in the extrathoracic region. *Aerosol Sci. Technol.*  
22 2003;37:659–671.
- 23 [51] Otto G. R, Yeh H, Schum GM, et al. *Tracheobronchial Geometry: Human, Dog, Rat,*  
24 *Hamster - A Compilation of Selected Data from the Project Respiratory Tract*  
25 *Deposition Models.* US Gov. Print. Off. 1976;
- 26 [52] Haefeli- Bleuer B, Weibel ER. Morphometry of the human pulmonary acinus. *Anat.*  
27 *Rec.* 1988;220:401–414.
- 28 [53] Colthorpe P, Voshaar T, Kieckbusch T, et al. Delivery characteristics of a low-  
29 resistance dry-powder inhaler used to deliver the long-acting muscarinic antagonist  
30 glycopyrronium. *J. Drug Assess.* 2013;2:11–16.
- 31 [54] Miller DP, Tan T, Nakamura J, et al. Physical Characterization of Tobramycin  
32 Inhalation Powder: II. State Diagram of an Amorphous Engineered Particle  
33 Formulation. *Mol. Pharm.* 2017;14:1950–1960.
- 34 [55] Pomázi A, Ambrus R, Szabó-Révész P. Physicochemical stability and aerosolization  
35 performance of mannitol-based microcomposites. *J. Drug Deliv. Sci. Technol.*  
36 2014;24:397–403.

1 [56] Lewis D, Rouse T, Singh D, et al. Defining the ‘Dose’ for Dry Powder Inhalers: The  
2 Challenge of Correlating In-Vitro Dose Delivery Results with Clinical Efficacy  
3 [Internet]. 2017 [cited 2018 Jul 12]. Available from:  
4 [https://www.americanpharmaceuticalreview.com/Featured-Articles/337338-Defining-](https://www.americanpharmaceuticalreview.com/Featured-Articles/337338-Defining-the-Dose-for-Dry-Powder-Inhalers-The-Challenge-of-Correlating-In-Vitro-Dose-Delivery-Results-with-Clinical-Efficacy/)  
5 [the-Dose-for-Dry-Powder-Inhalers-The-Challenge-of-Correlating-In-Vitro-Dose-](https://www.americanpharmaceuticalreview.com/Featured-Articles/337338-Defining-the-Dose-for-Dry-Powder-Inhalers-The-Challenge-of-Correlating-In-Vitro-Dose-Delivery-Results-with-Clinical-Efficacy/)  
6 [Delivery-Results-with-Clinical-Efficacy/](https://www.americanpharmaceuticalreview.com/Featured-Articles/337338-Defining-the-Dose-for-Dry-Powder-Inhalers-The-Challenge-of-Correlating-In-Vitro-Dose-Delivery-Results-with-Clinical-Efficacy/).

7 [57] Arpagaus C, Schafroth N, Meur M. Laboratory scale spray drying of lactose: A review  
8 [Internet]. 2010 [cited 2018 Jul 13]. Available from:  
9 <https://www.buchi.com/en/content/laboratory-scale-spray-drying-lactose-review>.

10

11

1 **Table 1. Compositions of the DPI formulations containing the applied concentration of**  
 2 **excipients.**

<b>Products</b>	<b>CIP [w/w %]</b>	<b>NaSt [w/w %]</b>	<b>IH 70 [w/w %]</b>	<b>MgSt [w/w %]</b>
$\mu$ CIP+IH70	9.09	-	90.91	-
CIP_0.5NaSt_spd	99.50	0.50	-	-
CIP_0.5NaSt_spd +IH70_MgSt	9.045	0.045	88.91	2.00

3

4 **Table 2. Residual solvent content in the samples.**

<b>Products</b>	<b>Residual solvent content (%)</b>	
	<b>Before storage</b>	<b>1 month</b>
$\mu$ CIP+IH70	0.492 $\pm$ 0.009	0.518 $\pm$ 0.006
CIP_0.5NaSt_spd	0.175 $\pm$ 0.002	0.218 $\pm$ 0.110
CIP_0.5NaSt_spd+IH70_MgSt	0.500 $\pm$ 0.005	0.490 $\pm$ 0.003

5



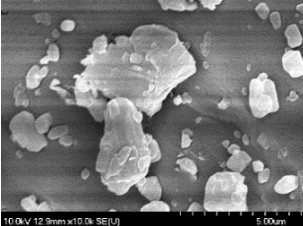
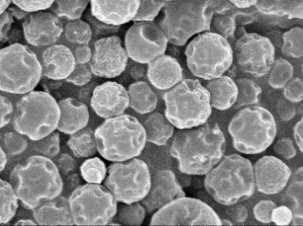
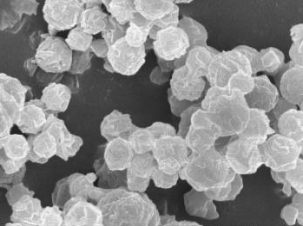
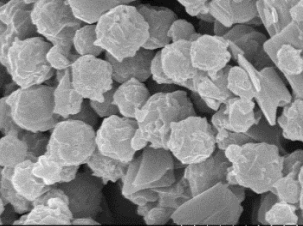
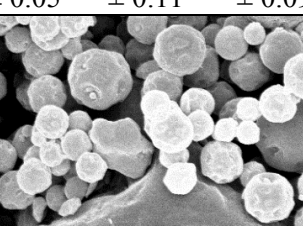
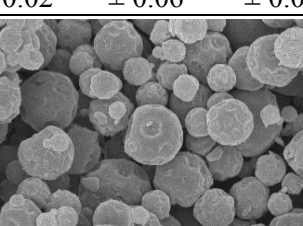
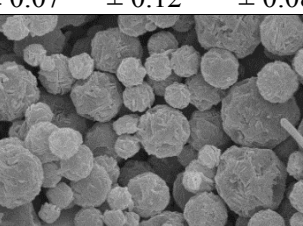
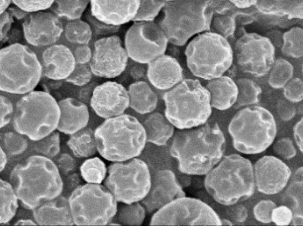
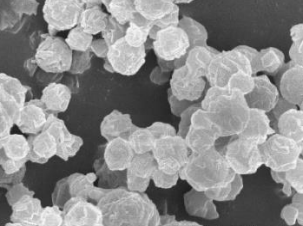
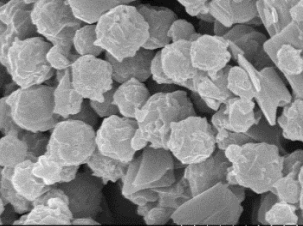
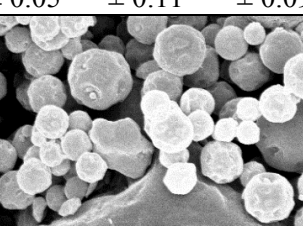
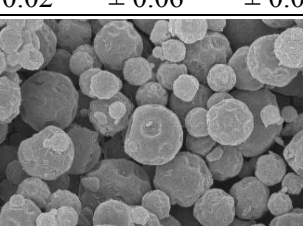
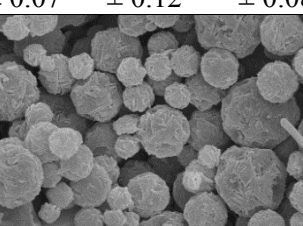
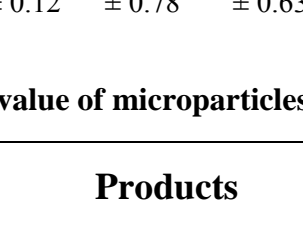
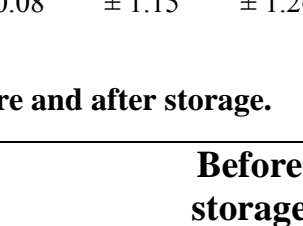
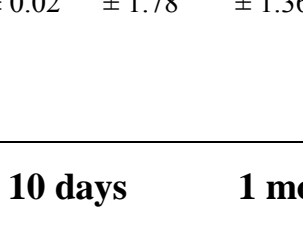
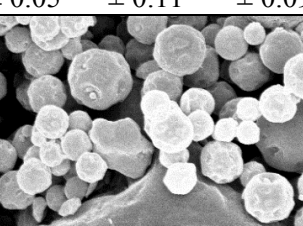
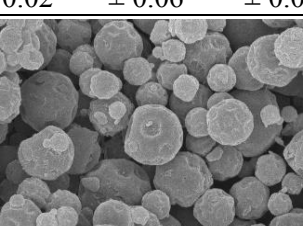
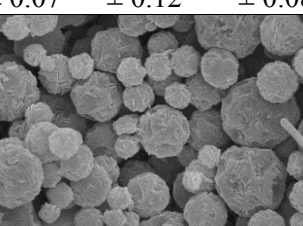
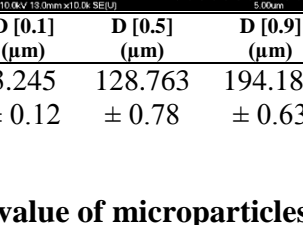
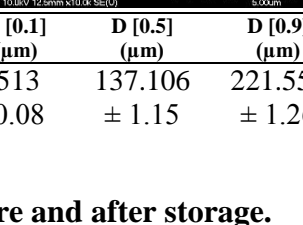
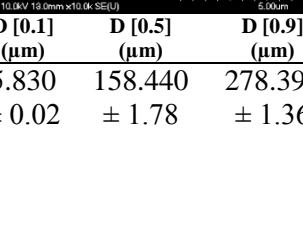
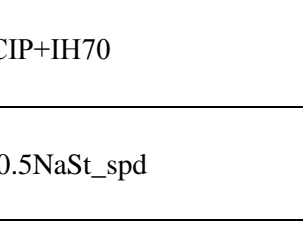
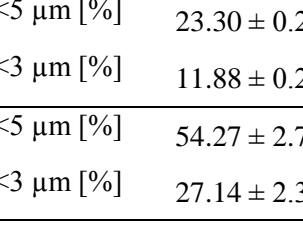
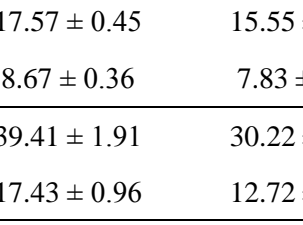
6 **Table 3. Cohesion, adhesion values and spreading coefficient of the preparations.**

<b>Products</b>	<b>W<sub>c</sub> [mN/m]</b>		<b>W<sub>adh</sub> [mN/m]</b>		<b>F<sub>adh</sub> [mN]</b>		<b>S<sub>21</sub></b>	
	<b>Before storage</b>	<b>1 month</b>	<b>Before storage</b>	<b>1 month</b>	<b>Before storage</b>	<b>1 month</b>	<b>Before storage</b>	<b>1 month</b>
$\mu$ CIP	161.60 $\pm$ 0.26	160.06 $\pm$ 0.66	-	-	-	-	-	-
$\mu$ CIP+IH70	-	-	108.26 $\pm$ 0.56	107.39 $\pm$ 0.77	1.690 *10 <sup>-3</sup> $\pm$ 0.09*10 <sup>-3</sup>	1.677 *10 <sup>-3</sup> $\pm$ 0.15*10 <sup>-3</sup>	1.64 $\pm$ 0.08	2.38 $\pm$ 0.13
CIP_0.5NaSt_spd	123.26 $\pm$ 0.89	144.74 $\pm$ 1.13	-	-	-	-	-	-
CIP_0.5NaSt_spd +IH70_MgSt	-	-	72.57 $\pm$ 1.26	81.81 $\pm$ 0.98	0.504 *10 <sup>-3</sup> $\pm$ 0.11*10 <sup>-3</sup>	0.593 *10 <sup>-3</sup> $\pm$ 0.07*10 <sup>-3</sup>	-19.06 $\pm$ 0.23	-49.1 $\pm$ 0.36

7

8

1 **Table 4. Morphology and particle size distribution of the formulations during the**  
 2 **storage.**

Products	Before storage			10 days			1 month		
$\mu$ CIP+IH70									
	D [0.1] ( $\mu$ m)	D [0.5] ( $\mu$ m)	D [0.9] ( $\mu$ m)	D [0.1] ( $\mu$ m)	D [0.5] ( $\mu$ m)	D [0.9] ( $\mu$ m)	D [0.1] ( $\mu$ m)	D [0.5] ( $\mu$ m)	D [0.9] ( $\mu$ m)
	15.034 $\pm$ 0.16	156.028 $\pm$ 1.85	198.152 $\pm$ 1.73	25.550 $\pm$ 0.26	170.366 $\pm$ 0.86	257.835 $\pm$ 1.19	31.846 $\pm$ 0.22	180.277 $\pm$ 1.81	285.720 $\pm$ 1.36
CIP_0.5NaSt_spd									
	D [0.1] ( $\mu$ m)	D [0.5] ( $\mu$ m)	D [0.9] ( $\mu$ m)	D [0.1] ( $\mu$ m)	D [0.5] ( $\mu$ m)	D [0.9] ( $\mu$ m)	D [0.1] ( $\mu$ m)	D [0.5] ( $\mu$ m)	D [0.9] ( $\mu$ m)
	1.208 $\pm$ 0.05	2.364 $\pm$ 0.11	4.556 $\pm$ 0.09	1.494 $\pm$ 0.02	2.466 $\pm$ 0.06	5.321 $\pm$ 0.04	1.608 $\pm$ 0.07	2.981 $\pm$ 0.12	23.123 $\pm$ 0.08
CIP_0.5NaSt_spd +IH70_MgSt									
	D [0.1] ( $\mu$ m)	D [0.5] ( $\mu$ m)	D [0.9] ( $\mu$ m)	D [0.1] ( $\mu$ m)	D [0.5] ( $\mu$ m)	D [0.9] ( $\mu$ m)	D [0.1] ( $\mu$ m)	D [0.5] ( $\mu$ m)	D [0.9] ( $\mu$ m)
	3.245 $\pm$ 0.12	128.763 $\pm$ 0.78	194.180 $\pm$ 0.63	4.513 $\pm$ 0.08	137.106 $\pm$ 1.15	221.555 $\pm$ 1.26	5.830 $\pm$ 0.02	158.440 $\pm$ 1.78	278.396 $\pm$ 1.36

3

4 **Table 5. FPF value of microparticles before and after storage.**

Products		Before storage	10 days	1 month
$\mu$ CIP+IH70	FPF <5 $\mu$ m [%]	23.30 $\pm$ 0.23	17.57 $\pm$ 0.45	15.55 $\pm$ 0.36
	FPF <3 $\mu$ m [%]	11.88 $\pm$ 0.20	8.67 $\pm$ 0.36	7.83 $\pm$ 0.18
CIP_0.5NaSt_spd	FPF <5 $\mu$ m [%]	54.27 $\pm$ 2.75	39.41 $\pm$ 1.91	30.22 $\pm$ 1.82
	FPF <3 $\mu$ m [%]	27.14 $\pm$ 2.38	17.43 $\pm$ 0.96	12.72 $\pm$ 1.66
CIP_0.5NaSt_spd+IH70_MgSt	FPF <5 $\mu$ m [%]	63.75 $\pm$ 1.21	57.36 $\pm$ 2.21	47.12 $\pm$ 0.78
	FPF <3 $\mu$ m [%]	39.22 $\pm$ 0.74	33.56 $\pm$ 0.96	26.52 $\pm$ 1.12

5

6

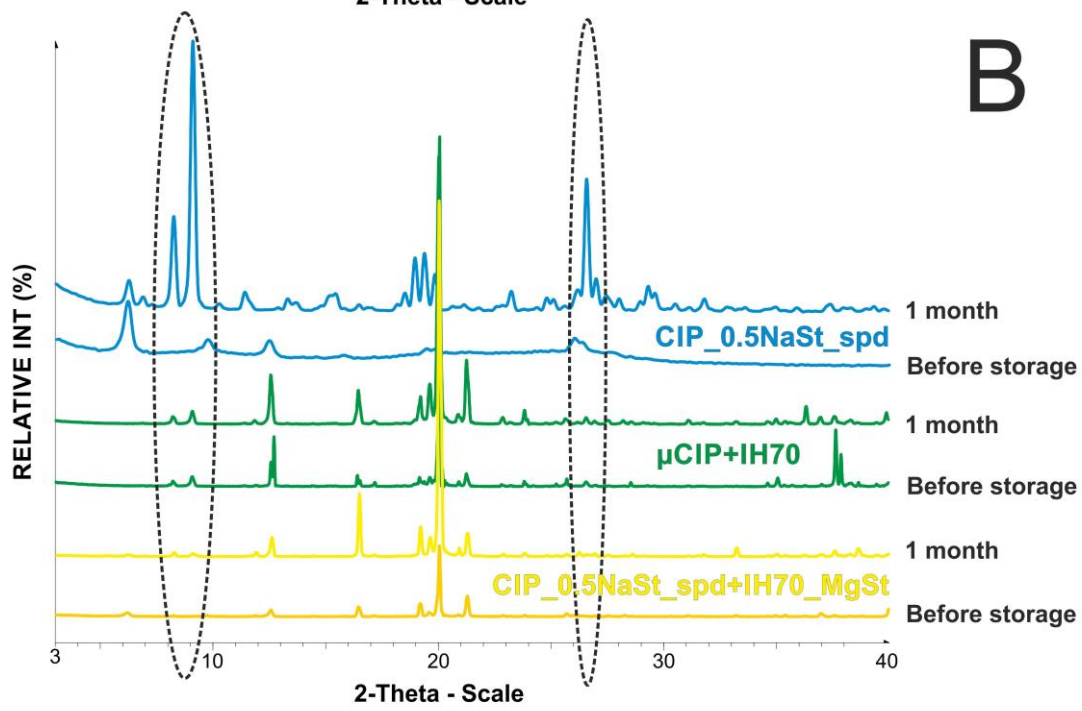
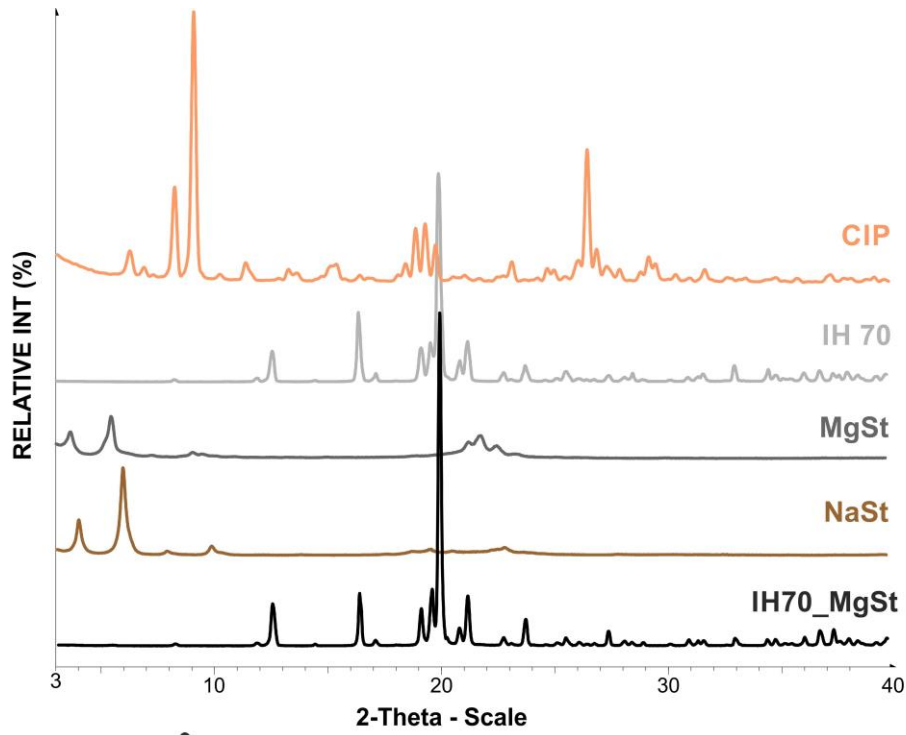
1 **Table 6. EF and MMAD values of microparticles before and after storage.**

<b>Products</b>		<b>Before storage</b>	<b>10 days</b>	<b>1 month</b>
$\mu$ CIP+IH70	EF [%]	96.92 $\pm$ 0.11	95.56 $\pm$ 0.22	96.52 $\pm$ 0.45
	MMAD [ $\mu$ m]	7.98 $\pm$ 0.10	10.02 $\pm$ 0.15	11.40 $\pm$ 0.23
CIP_0.5NaSt_spd	EF [%]	76.99 $\pm$ 3.32	92.23 $\pm$ 0.21	92.32 $\pm$ 0.19
	MMAD [ $\mu$ m]	4.14 $\pm$ 0.18	5.48 $\pm$ 0.28	6.54 $\pm$ 0.05
CIP_0.5NaSt_spd+IH70_MgSt	EF [%]	90.45 $\pm$ 1.80	90.65 $\pm$ 0.32	89.46 $\pm$ 1.12
	MMAD [ $\mu$ m]	3.47 $\pm$ 0.02	4.03 $\pm$ 0.19	5.47 $\pm$ 0.35

2

3

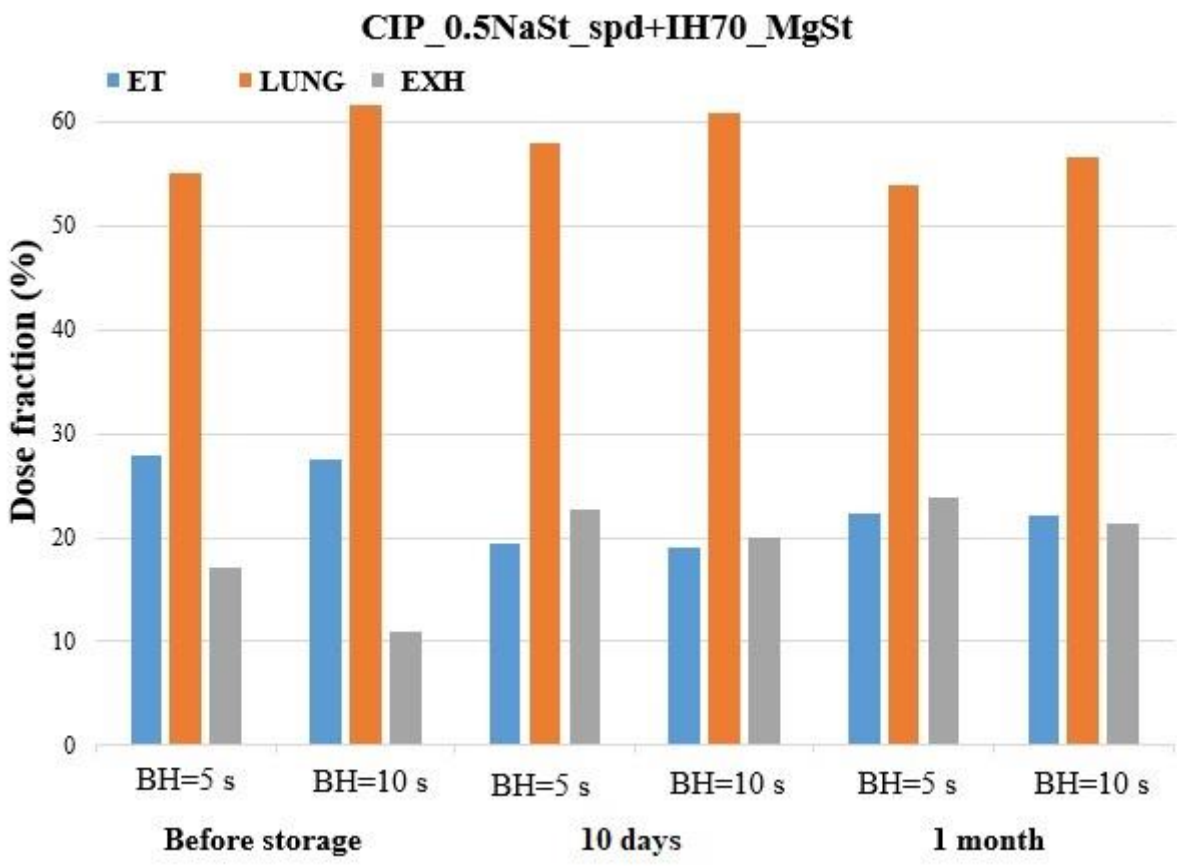
4



1  
2  
3  
4  
5  
6  
7  
8

Figure 1.

1  
2  
3  
4  
5  
6



7  
8  
9

Figure 2